Neoproterozoic-hosted Carlin-type mineralization in central Yukon, part 1: Regional- to prospect-scale geological controls

Nicolas Pinet[1]*, Patrick Sack[2], Patrick Mercier-Langevin[1], Maurice Colpron[2], Denis Lavoie[1], Benoît Dubé[1], and Virginia I. Brake[1]

[1]Geological Survey of Canada, 490 rue de la Couronne, Québec, Quebec G1K 9A9
[2]Yukon Geological Survey, 91807 Alaska Hwy, Whitehorse, Yukon Y1A 5B7
*Corresponding author's e-mail: nicolas.pinet@canada.ca

ABSTRACT

In central Yukon, sediment-hosted gold mineralized zones have similar characteristics to Carlin-type deposits in Nevada. However, it remains unclear if exploration models applied to the southwest United States similarly apply to the Canadian Cordillera. This contribution tackles that knowledge gap by reviewing the regional- to prospect-scale setting of mineralized zones found in the Nadaleen trend, Yukon. Carlin-type gold-bearing zones in central Yukon are located near the boundary between the Ogilvie platform to the northeast and the Selwyn Basin to the southwest. This shelf-to-basin transition is marked in part by the Dawson fault, which is likely a long-lived, deep-seated structure that influenced sedimentation and younger structural history. Gold-mineralized zones are mainly hosted in two Neoproterozoic limestone units (informally known as the Conrad and Osiris limestones of the Nadaleen and Gametrail formations, respectively) and in Paleozoic siltstones. In the Nadaleen trend, the structural style is complex; the strata generally dip more steeply than in classic fold-and-thrust belts and faults bear a significant strike-slip component. Neoproterozoic-hosted gold ore zones are mostly concordant with bedding in complexly shaped anticlines. Gold mineralization is significantly younger than the main intrusion-related gold mineralizing event in the northern Selwyn Basin.

INTRODUCTION

Globally, Carlin-type deposits represent a major source of gold and one of the principal exploration targets due to their potential to form districts with large gold content. The vast majority of known Carlin-type gold deposits are located in Nevada, where they are defined by their common tectono-sedimentary setting, geochemical/mineralogical signature, and timing (Table 1; Cline et al., 2005; Muntean, 2018a). In Nevada, the huge gold endowment (~255 Moz: Muntean, 2018a) within Carlin-type deposits resulted from (1) geological processes spanning hundreds of millions of years that led to an ideal crustal architecture at regional- to drill-target scales (ground preparation); and (2) a relatively short-lived geodynamic event that modified the thermal state and tectonic regime of the lithosphere, which resulted in a change from shortening to extension and renewed magmatism. Studies of the few Carlin-type occurrences found outside the Great Basin of the southwest United States are limited (Muntean, 2018b and references therein), and it remains unclear if the geological processes/geodynamic events documented in Nevada are absolute prerequisites to generate Carlin-type deposits. This is important for mineral exploration because it impacts whether geological and exploration models developed in Nevada can be applied elsewhere. In this study, we tackle this knowledge gap by reviewing geological parameters that may have been critical in forming Carlin-type gold mineralization in central Yukon at the lithospheric to prospect scales (100s of kms to 100s of ms). A companion study (Pinet et al., 2020) documents the critical ore-forming processes at the drill-target scale and below (≤100 m).

REGIONAL SETTING

Geological Framework

In Yukon and Northwest Territories, the foreland belt forms the easternmost geological domain of the Cordilleran orogen. The foreland belt consists of sedimentary rocks deposited on the Laurentian (North American) continental margin, which is tectonically juxtaposed to the west against a variety of allochthonous lithotectonic assemblages. Each of these lithotectonic terranes was accreted to ancestral North America during the Mesozoic (Nelson et al., 2013).

Northeast of the Tintina fault, a major strike-slip fault with 430 km of Eocene and a further 60 km of Late Cretaceous right lateral displacement (Gabrielse et al., 2006), the foreland belt exhibits an arcuate geometry with salients and recesses characterized by different tectonic styles (Fig. 1). In the Mackenzie

Pinet, N., Sack, P., Mercier-Langevin, P., Colpron, M., Lavoie, D., Dubé, B., and Brake, V.I., 2020. Neoproterozoic-hosted Carlin-type mineralization in central Yukon, part 1: Regional- to prospect-scale geological controls; *in* Targeted Geoscience Initiative 5: Contributions to the Understanding of Canadian Gold Systems, (ed.) P. Mercier-Langevin, C.J.M. Lawley, and S. Castonguay; Geological Survey of Canada, Open File 8712, p. 281–297. https://doi.org/10.4095/326045

Table 1. Selected geological characteristics of Carlin-type deposits in Nevada.

Tectono-sedimentary setting
Host rock characterized by significant carbonate content
Location in the lower plate of a pre-ore regional thrust
Association with extensional faults and pre-ore contractional structures
Depth of formation <3 km
Geochemical/mineralogical signature
Pathfinder elements Tl, As, Hg, Sb
Low Ag and base metal content
Alteration characterized by decarbonatization, silicification, and argillitization
'Invisible' gold in arsenian pyrite either as rims on pre-ore pyrite or as sub-micrometre particles
Minor open-space filling minerization
210 ± 30°C low-salinity main ore-stage fluids
Timing
Narrow age range between 42 and 34 Ma

Mountains (Fig. 1a), shortening (~50 km) was accommodated by east- and west-verging folds and thrusts that trend parallel to the north-trending deformation front (Gordey, 1981). This contrasts with the deformation style of the northern boundary of the most pronounced salient, where major faults trend west-northwest (Fig. 1b). Among these faults, the 250 km long Dawson fault was a first-order structure during the Mesozoic building of the Cordillera (Abbott, 1997). However, evidence suggests that the fault is a deep-seated structure originating from older tectonic events.

1. The present-day location of the Dawson fault roughly coincides with the northern boundary of the Selwyn Basin (Fig. 1b), a domain with Neoproterozoic to Permian sedimentary rocks mainly deposited in basinal settings and characterized by deeper water sediments than the surrounding platform domains. Paleogeographic reconstructions (Cecile, 1982) indicate that the Ogilvie Platform-Selwyn Basin transition was relatively stable from the Cambrian to the Silurian and located close to the inferred Neoproterozoic platform-basin boundary (Abbott, 1997).
2. Mass-transport deposits most likely associated with syndepositional tectonism are ubiquitous in the Neoproterozoic to mid-Paleozoic sedimentary successions that are present near the Ogilvie Platform-Selwyn Basin transition, reinforcing the idea of a long-lived structurally controlled, south-facing (present coordinates) slope.
3. Kilometre-scale ultramafic bodies, possibly linked with the transform fault transition from the upper plate to the lower plate segments along the continental margin, are present along the Dawson fault system (Colpron, 2012).
4. Several occurrences of Cambrian, Silurian, and Devonian Paleozoic igneous rocks, including basalt, rhyolite and gabbro, are documented in the northern part of the Selwyn Basin. These are particularly notable in the vicinity of the Dawson fault (Yukon Geological Survey, 2019).

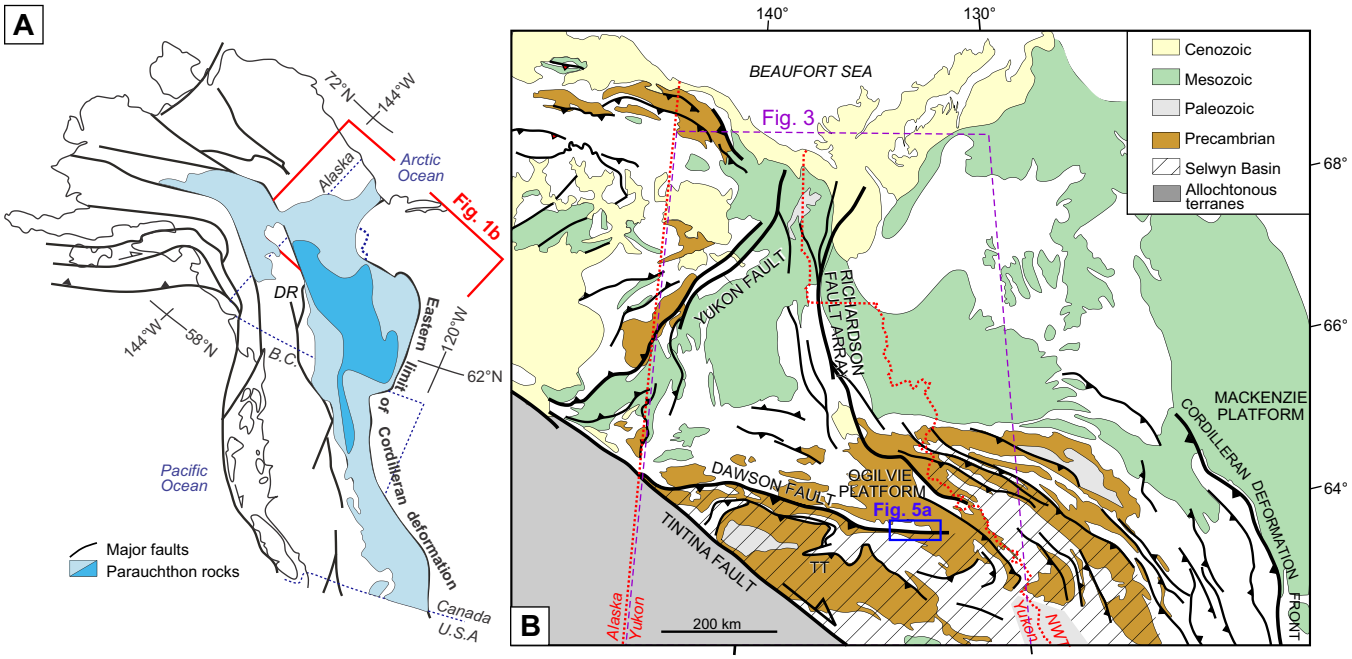

Figure 1. a) Simplified geological map of the northern Cordillera in Canada and Alaska. Parautochthonous rocks include basinal (darker blue) and platformal (lighter blue) strata. Abbreviations: DR = Dawson Range, MM = Mackenzie Mountains, OP = Olgilvie Platform, SB = Selwyn Basin. **b)** Geological map of the foreland belt in northern Yukon and Northwest Territories. Note the changes in strike of the major faults. Abbreviation: TT = Tombstone Thrust.

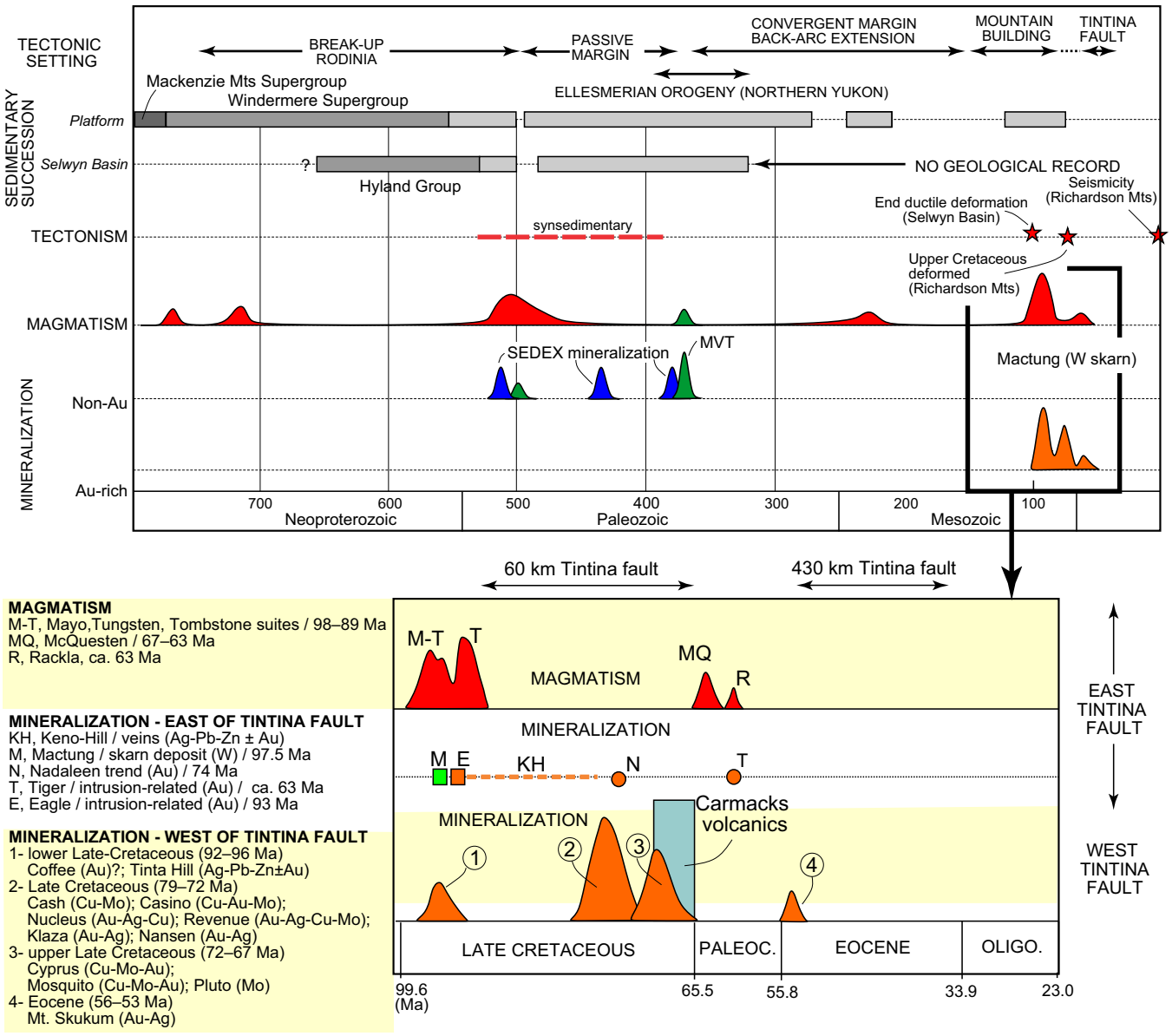

Figure 2. Schematic geological timeframe of north-central Yukon. For clarity, only the Windermere Supergroup and Hyland Group are distinguished (medium grey). Abbreviations: MVT = Mississippi Valley-type, SEDEX = sedimentary exhalative. Ages of magmatism from Murphy (1997), Hart et al. (2004a,b), Kingston et al. (2010), Rasmussen (2013), and Colpron et al. (2016). Ages of mineralization from Selby and Creaser (2001), Allan et al. (2013), Bineli Betsi et al. (2013), Nelson et al. (2013), Mortensen et al. (2016), and Davis et al. (2019).

Due to the lack of post-Permian rocks, the age and kinematics of Cordilleran deformation events that affected the Ogilvie Platform-Selwyn Basin boundary remain poorly constrained. In the western segment of the platform-basin boundary, ductile fabrics associated with the Tombstone thrust (Fig. 1b) are post-Jurassic, but pre-95 Ma, as they are intruded by Late Cretaceous plutons (Murphy, 1997). Brittle faults and open folds are superimposed on ductile fabrics, but their timing is poorly constrained. North of the Selwyn Basin, Cenozoic to Quaternary deformation is documented along the Yukon fault and the Richardson fault array (Fig. 1a; Jeletzky, 1961; Mazotti and Hyndman, 2002).

Most of the Mesozoic intrusive rocks in the northern Selwyn Basin belong to three early Late Cretaceous (98–89 Ma) magmatic suites (i.e. Mayo, Tungsten, and Tomstone suites, with dominantly metaluminous, peraluminous, and alkali characteristics, respectively; Hart et al., 2004a,b; Rasmussen, 2013) and to the volumetrically less important latest Cretaceous to earliest Paleocene (67–63 Ma) McQuesten suite (Fig. 2; Murphy, 1997; Rasmussen, 2013; Colpron et al., 2016).

Geophysical Framework

In northern Yukon and Northwest Territories, the residual total magnetic field is dominated by the high-

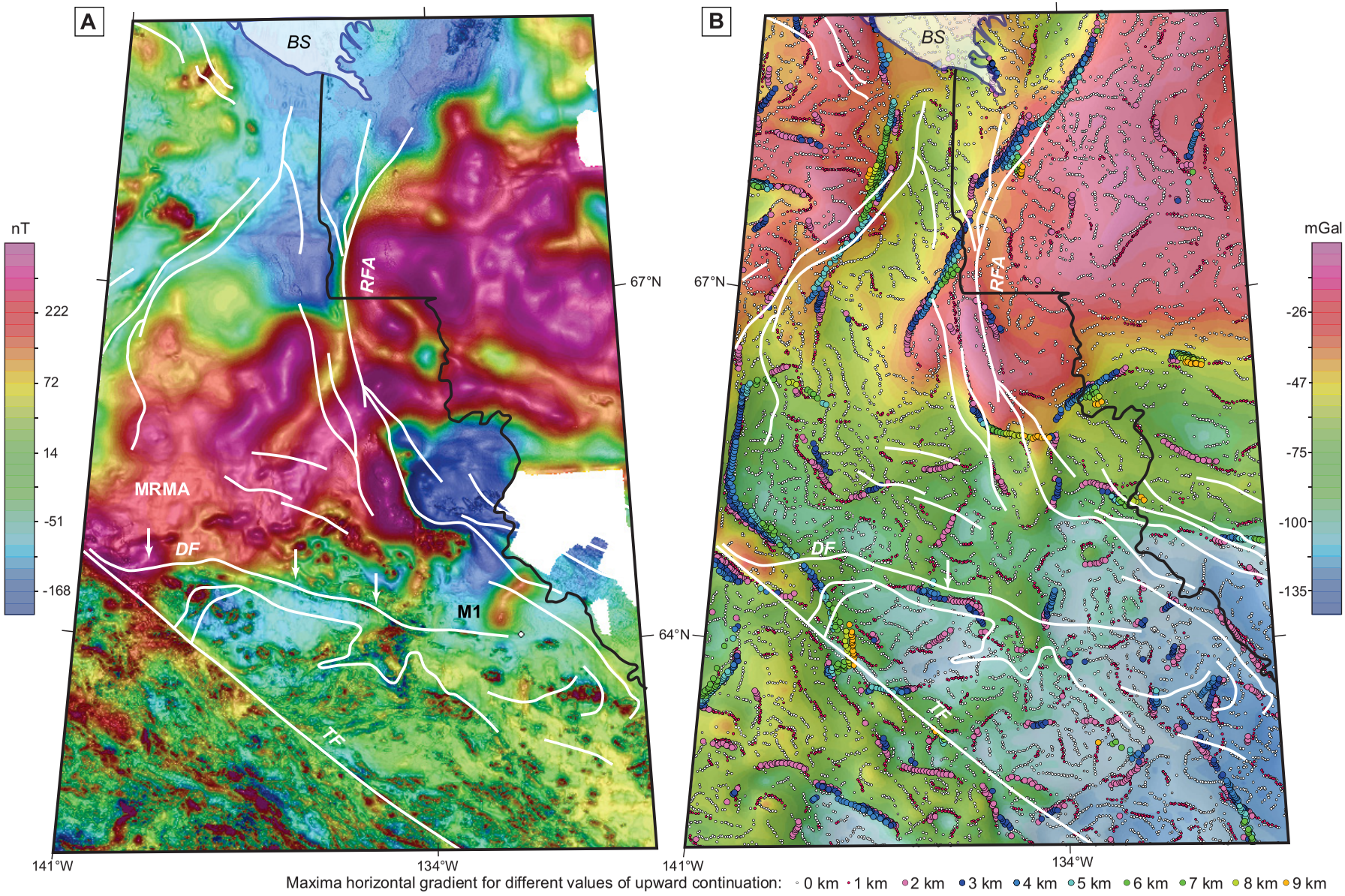

Figure 3. Residual total magnetic field **(a)** and Bouguer anomaly **(b)** over northern Yukon and Northwest Territories (*see* Fig. 1 for location). In (a), M1 is a magnetic anomaly that is discussed in the text. In (b), the points correspond to the maxima of the horizontal gradient for different values (0–9 km) of upward continuation and have been generated for this study. The maxima represent a way to automatically map the density contrast boundaries. White lines represent the regional faults. White arrows indicate major geophysical features associated with the Dawson fault. Abbreviation: BS = Beaufort Sea, DF = Dawson fault, MRMA = Mackenzie River magnetic anomaly, RFA = Richardson fault array, TF = Tintina fault.

amplitude, long-wavelength Mackenzie River magnetic anomaly (Fig. 3a) interpreted to be associated with Early Proterozoic magmatic arc crust at depth (Pilkington and Saltus, 2009). In Yukon, the southern boundary of the anomaly strikes west-northwest and is coincident with the western segment of the Dawson fault (Fig. 3). Regional seismic tomography models that map seismic velocity anomalies (dv/v; Fig. 4) is another tool to study the lithospheric architecture of the area. The low resolution of the regional tomographic image prevents the mapping of individual structures (such as the Dawson fault). However, the tomographic cross-section generated for this study and presented on Figure 4 clearly shows the juxtaposition of lithospheric domains with seismic waves propagating slightly faster (to the north) or slower (to the south) than average ambient mantle or crust, which correlate with density, temperature, and/or compositional variations (Kennett et al., 1995). This tomographic section substantiates the interpretation in which the northern boundary of the Selwyn Basin is a major structural break at the lithospheric scale.

Gravity stations in northern Yukon are typically located between 10 and 15 km apart, which prevents a detailed analysis of subtle gravity features. However, the western segment of the Dawson fault is marked by gravity gradients >1 mGal/km and is clearly defined by the linear distribution of maxima of the horizontal gravity gradient (white arrows on Fig. 3b). Similar to that of the magnetic data (Fig. 3a), the gravity signature of the eastern segment of the fault is more subtle, in agreement with geological evidence indicating that the fault splits into several branches to the east (*see below*).

Regional Metallogeny

In northern Yukon, the styles and ages of mineralization range from Proterozoic syngenetic deposits to Cenozoic epigenetic deposits (Nelson et al., 2013).

North of the Selwyn Basin-Ogilvie Platform boundary, mineralization is Precambrian and includes the following: 1) the Paleoproterozoic Cu-Au-U-Co-enriched Wernecke breccia (Thorkelson et al., 2001); 2) the Mesoproterozoic Hart River massive sulphide deposit; and 3) the Neoproterozoic Crest Fe deposit hosted by the glaciogenic strata of the Rapitan Group (Yeo, 1986).

In the northern Selwyn Basin, disparate mineralization styles broadly coincide with specific time periods (Fig. 2). Paleozoic mineralization consists largely of Zn-Pb±Ag sedimentary-exhalative-type occurrences that formed in mid-Cambrian (Anvil district: Pigage, 2004), early Silurian (Howards Pass district: Goodfellow and Jonasson, 1986) and Late Devonian (Macmillan Pass: Magnall et al., 2014). Although of lesser significance, Late Devonian–Mississippian poly-

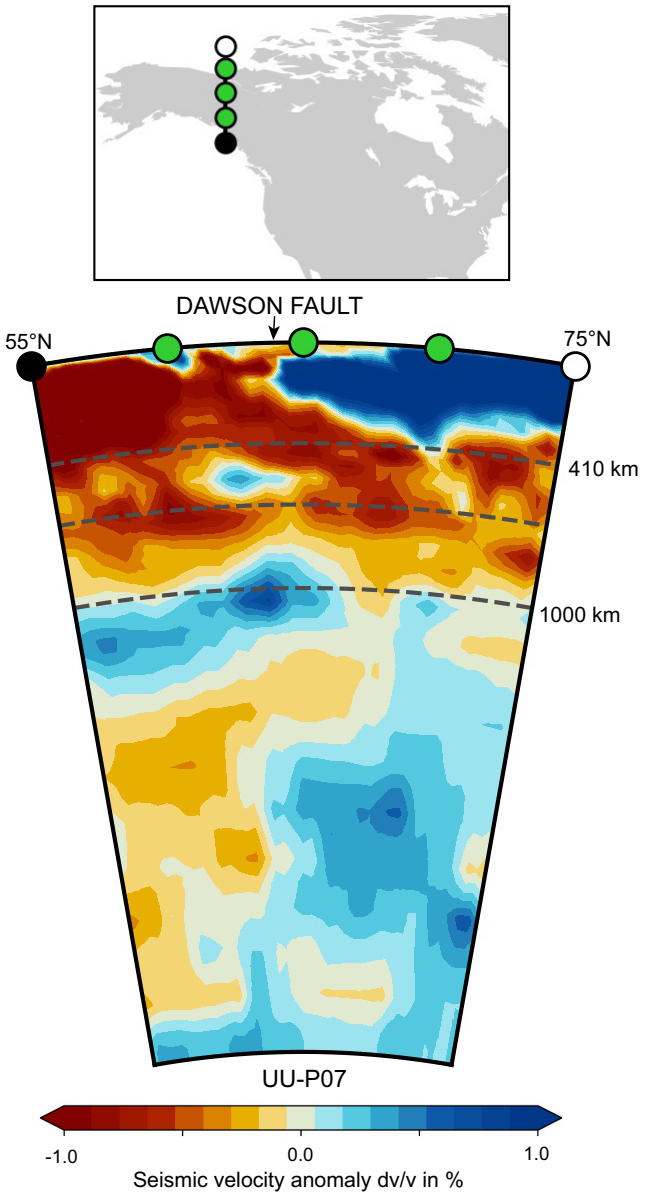

Figure 4. A tomographic image across the northern Cordillera, which has been generated for this contribution from the UU-P07 model (Amaru, 2007).

metallic, volcanogenic massive sulphide deposits also occur in Selwyn Basin and Mississippi Valley-type Zn-Pb occurrences in the Mackenzie Platform to the east are thought to be mainly mid-Paleozoic (Nelson et al., 2002).

Mesozoic mineralization in the northern Selwyn Basin region defines the eastern part of the Tintina gold province (Hart et al., 2004a,b), a regional belt of mineralization spatially and temporally associated with the early Late Cretaceous Tungsten (98–95 Ma), Mayo (98–93 Ma) and Tombstone (93–89 Ma) magmatic suites (Fig. 2). It includes the reduced intrusion-related Au deposits at Dublin Gulch, Clear Creek, Scheelite Dome, and Brewery Creek (Maloof et al., 2001; Marsh et al., 2003; Hart et al., 2004a,b; Lindsay, 2006; Mair et

al., 2011). Farther to the east, close to the boundary with Northwest Territories, the Mactung world-class W skarn deposit is also early Late Cretaceous. Quartzite-hosted polymetallic Ag-Pb-Zn veins of the Keno Hill district (Cathro, 2006) are classically associated with the Tombstone plutonic suite (e.g. Sinclair et al., 1980), but unpublished $^{40}Ar/^{39}Ar$ dating of mica suggests a possible Late Cretaceous age (Cragg, pers. comm., 2019), possibly related to nearby small intrusions of the McQuesten plutonic suite (ca. 67–63 Ma: Murphy, 1997; Colpron et al., 2016).

The youngest metallogenic event is upper Late Cretaceous to Eocene (?). East of the Tintina fault, it is documented only in the Rackla belt, a 5–15 km wide fold-and-fault belt bounded to the north by the Kathleen Lakes fault and to the south by the Dawson fault. The Rackla belt includes the Rau trend to the west and the Nadaleen trend to the east (Fig. 5a). The Rau trend consists of the Tiger deposit and a series of sediment-hosted occurrences that are still at an early stage of exploration. Sulphide replacement of Silurian carbonate rocks at the Tiger deposit (Thiessen et al., 2016) is linked to an intrusion that yielded Ar-Ar muscovite cooling ages between 62.3 and 59.1 Ma (Kingston et al., 2010). The Nadaleen trend consists of a series of Carlin-type gold mineralized zones (Arehart et al., 2013; Tucker et al., 2018) that are the focus of this study as well as auriferous quartz veins and sediment-hosted occurrences.

In the Nadaleen trend, U-Pb zircon dating from a locally gold-mineralized dyke indicates that the age of mineralization is <74 Ma (Tucker, 2015; Tucker et al., 2018). During the present study, late ore-stage calcite has been dated by U-Pb laser ablation inductively-coupled plasma mass spectrometry (LA-ICP-MS). Preliminary results reported in Davis et al. (2019) show variable degrees of complexity. Samples from the Conrad zone (n = 3) yield a relatively simple age distribution, including Tera-Wasserburg intercept ages between 72 and 75 Ma. Samples from the Osiris/Sunrise zone (n = 2) are significantly more complex and yield scattered U-Pb ages that may reflect several hydrothermal events, including one at ca. 73 Ma and one or several younger events. The relationship between these hydrothermal pulses and gold-mineralization is still under investigation.

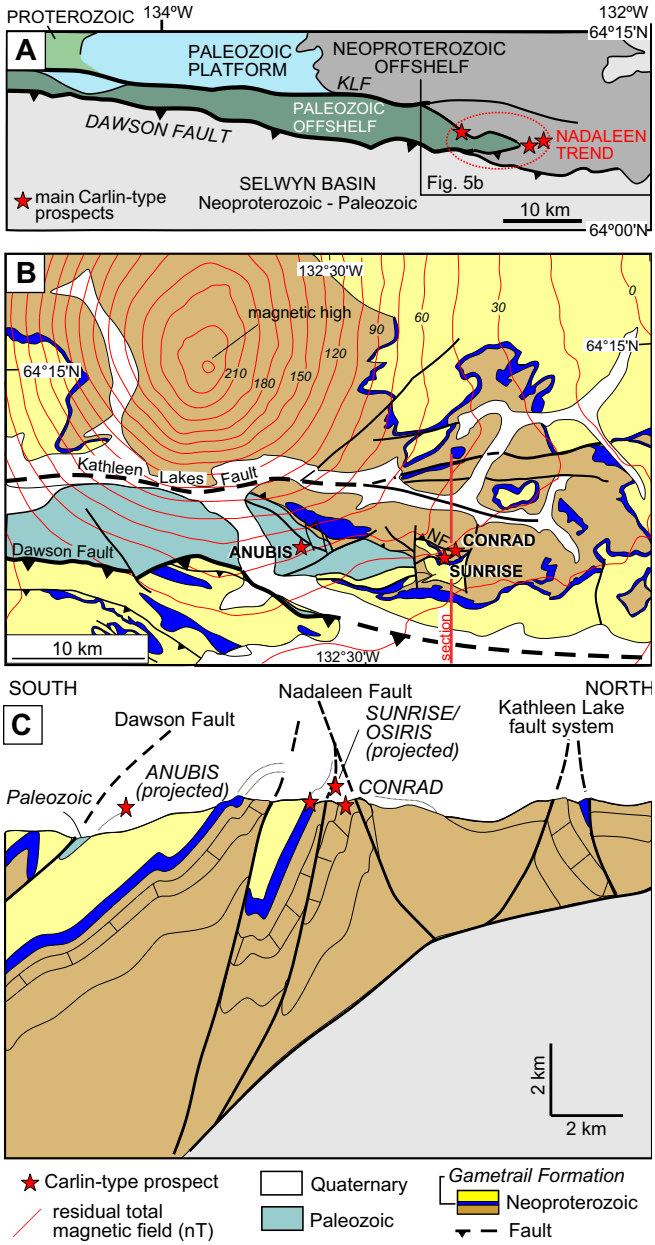

Figure 5. a) Simplified geological map of the eastern Rackla belt (*after* Colpron et al., 2013); abbreviation: KLF = Kathleen Lakes fault. **b)** Geological map (*modified from* Moynihan, 2016). Abbreviation: NF = Nadaleen fault. **c)** North-south cross-section, location of which is shown in (b).

DISTRICT-SCALE SETTING: THE EASTERN RACKLA BELT

Despite its remote location, our understanding of the geological setting of the eastern Rackla belt has been recently improved through active exploration in the area (e.g. Ristorcelli et al., 2018), a multiyear mapping project conducted by the Yukon Geological Survey (Fig. 5; Colpron et al., 2013; Moynihan, 2016) and thematic research (e.g. Arehart et al., 2013; Beaton, 2015; Tucker, 2015; Palmer and Kuiper, 2016 Pinet et al., 2018; Steiner et al., 2018; Tucker et al., 2018; Pinet and Sack, 2019).

Stratigraphic Framework

The eastern Rackla belt comprises a lithologically diverse Neoproterozoic to Permian sedimentary succession (Fig. 6). The Neoproterozoic part of the succession belongs to the upper parts of the Windermere Supergroup (Moynihan et al., 2019). The oldest rocks in the eastern Rackla belt are latest Cryogenian and

consist of predominantly fine to coarse clastic strata with some silty to sandy limestone of the Twitya and Ice Brook formations (both belonging to the Hay Creek Group). The recently defined Rackla Group (Moynihan et al., 2019) conformably overlies the Ice Brook Formation and includes (1) fine-grained clastic rocks (Sheepbed Formation); (2) a heterogeneous mixed siliciclastic and carbonate succession (Nadaleen Formation); (3) distinctive, cliff-forming limestone and dolostone (Gametrail Formation) characterized by a large negative carbon isotope excursion that is correlated with the 579–551 Ma Shuram anomaly (Macdonald et al., 2013, 2017); (4) fine-grained siliciclastic rock (with some carbonate intervals) and sandstone (Blueflower Formation); and (5) cliff-forming limestone (Algae Formation). The Neoproterozoic-Cambrian contact is marked by an irregular erosional surface at the contact with overlying varicoloured mudstone and siltstone (Cambrian Narchilla Formation). A few kilometres southeast of the map area shown in Figure 5b, Cambrian-Ordovician rocks correspond to boulder conglomerate, mudstone, and siltstone of the Gull Lake Formation and mafic volcaniclastic and fragmental volcanic rocks of the Old Cabin Formation (Moynihan, 2013). In the Anubis area (Fig. 5b), Paleozoic rocks form a 2–7 km wide syncline with mainly fine-grained siliciclastic (black shale and siltstone) intervals alternating with three carbonate units. Within the syncline, fossil assemblages range from Middle Ordovician to Early Permian (Moynihan, 2016).

The entire Neoproterozoic succession was deposited below wave base in slope-to-basin settings, with the possible exception of some flat-pebble conglomerate layers in the Gametrail Formation that may indicate an outer ramp or shelf setting (Moynihan et al., 2019). Evidence of soft sediment deformation is present in almost all Neoproterozoic formations and in some Paleozoic units and include slump intervals with discontinuous folds and/or basal shears and flame structures.

Tectonic Framework

The Rackla belt is bounded by the Dawson fault to the south and the Kathleen Lakes fault to the north. Both faults split into several branches in the eastern Rackla belt. Some splays trend west-northwest, slightly oblique to the more east-west regional trend (Moynihan, 2016; Fig. 5b). As a result, displacements along individual faults tend to decrease toward the east and differences in the magnetic signature on both sides of faults are less apparent.

South of the Dawson fault, folds are generally tight and trend west-northwest- with a clear asymmetry to the north. In the Anubis area (Fig. 7a), the Dawson

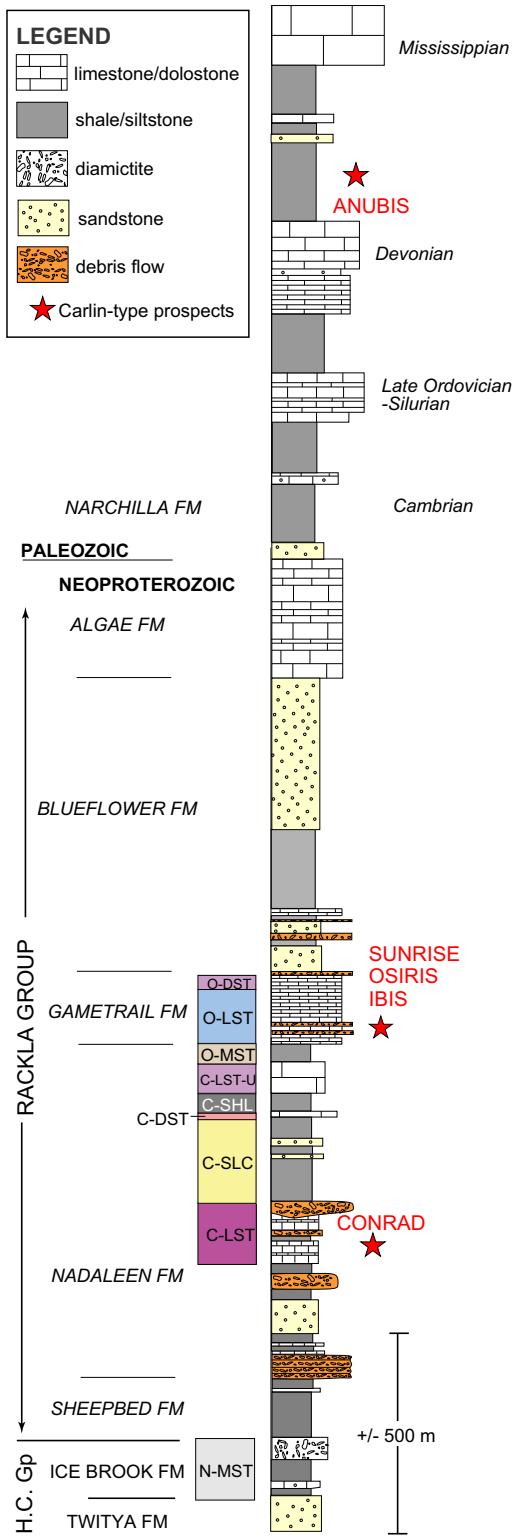

Figure 6. Sedimentary succession in the eastern Rackla belt, which has been *adapted from* Moynihan et al. (2019) for the Neoproterozoic. Informal sedimentary units are those cited in the text and are represented using the following abbreviations: C-DST = Conrad dolostone, C-CHL = Conrad shale, C-LST = Conrad limestone, C-LST-U = upper Conrad limestone, C-SLC = Conrad siliciclastic rock, H.C. Gp = Hay Creek Group, N-MST = NONAD mudstone, O-DST= Osiris dolostone, O-LST = Osiris limestone, O-MST = Osiris mudstone. Other abbreviation: FM = Formation.

fault is a moderately south-dipping structure that juxtaposes a >3 km succession of Neoproterozoic to Lower Cambrian rocks in its hanging wall upon Paleozoic strata in its footwall (Fig. 5, 7a).

North of the Dawson fault, fault dip direction and fold asymmetry vary. Fold interference is documented from regional (Moynihan, 2016) to outcrop scale (Steiner et al., 2018; this study). Regional west-northwest-trending folds predominate, some exhibiting an en échelon geometry relative to the Kathleen Lakes fault (Fig. 7a). Folds plunge either to the west-northwest or east-southeast and have a steeply dipping axial planar cleavage locally developed in fine-grained siliciclastic intervals. Faults trending obliquely to the east-west regional faults are common in the eastern Rackla belt (Fig. 7a). Northwest-striking faults are well developed throughout the area and generally exhibit a right-lateral component of displacement documented by the apparent offset of east-west-trending structures (including the Dawson fault) and magnetic markers on the high-resolution survey flown for ATAC Resources. A notable exception is the Osiris fault, which, despite trending east to east-northeast, is characterized by an apparent right-lateral sense of motion. It is likely that some of this apparent displacement reflects fault reactivation (*see below*). Some northeast-striking faults are also documented and exhibit a left-lateral component of displacement (Fig. 7a). Both northwest- and northeast-trending faults are compatible with a regime of left-lateral transpression (Fig. 7b). This regime is in agreement with the predominance of contractional structures and with the 10 km (northwest of Conrad) to 2.5 km (northeast of Conrad) left-lateral offset of steeply dipping contacts along the Kathleen Lakes fault (Fig. 7c,d; Moynihan, 2016). North of the Stewart River, regional mapping by Moynihan (2016) indicates that northeast-trending folds are also present in a restricted zone that includes the Osiris cluster. These anomalously trending folds are inconsistent with a model of left-lateral transpression and suggest that they formed in a distinct tectonic episode.

The structural complexity and polyphase structural history of the eastern Rackla belt are well exemplified by the scattering of bedding data on an equal-area lower-hemisphere stereodiagram (Fig. 7c), with a predominance of moderate to relatively steep dips (average 55°). Fault plane data collected during the course of this study are consistent with such structural complexity. Fault planes are generally steeply dipping and exhibit highly variable slickenline rakes attesting, in most cases, to mixed dip-slip (thrust or normal) and strike-slip (left- or right-lateral) components (Fig. 7d). In several cases, several generations (up to 3) of slickenlines are present on a single fault plane, demonstrating the polyphase structural history of the area. The relative timing of slickenlines is documented in a few cases only, preventing a detailed paleostress analysis.

LITHOSTRATIGRAPHY AND GEOMETRY OF THE NEOPROTEROZOIC-HOSTED GOLD MINERALIZED ZONES

The Nadaleen trend comprises several gold zones that are hosted in Neoproterozoic (Osiris cluster) and Paleozoic (Anubis cluster) rocks. This study focuses on the Conrad, Sunrise, and Osiris zones; the Ibis zone, also part of the Osiris cluster but located in the Osiris fault hanging wall (Fig. 8), has not been studied in detail.

Conrad Zone

The Neoproterozoic-hosted Conrad gold mineralized zone (Fig. 8) is the most intensively drilled (43,433 m in 108 holes) with inferred resources estimated at 9.7 Mt at 4.15 g/t (1.29 Moz Au: Ristorcelli et al., 2018). The Conrad area is poorly exposed. However, detailed mapping (Fig. 8) and drill data indicate that the main host unit (Conrad limestone, part of the Nadaleen Formation) forms the core of a doubly plunging anticline. The anticline is in fault-contact to the north and stratigraphic contact to the south with non-calcareous siliciclastic rocks with little evidence of paleofluid flow (veins), suggesting that siliciclastic rocks have low porosity and permeability. Mineralized intervals are documented for 800 m along strike and to a minimum vertical interval of 500 m (Ristorcelli et al., 2018).

The oldest sedimentary unit is found in the hanging wall of the Nadaleen fault, structurally overlying the Conrad mineralized zone (Fig. 8). It corresponds to varicoloured, thinly laminated mudstone and siltstone with quartz pebble conglomerate intervals. Evidence for soft-sediment deformation is common and pyrite (including locally cm-scale nodules) is disseminated throughout the unit. This unit, informally known as the NONAD mudstone, is regionally correlated with the Ice Brook Formation (Fig. 6; Moynihan et al., 2019).

In the footwall of the Nadaleen fault, the limestone unit is a medium grey lime mudstone/wackestone (Fig. 9a) with some intraclastic packstone (and minor grey to black siltstone). Limestone beds vary from a few millimetres to 20 cm (with a few beds >1 m) in thickness, and exhibit planar contacts. Cone-in-cone (Fig. 9b) and beef calcite are common and probably formed as hydraulic fractures through the degassing of biogenic methane during shallow burial (Meng et al., 2017), suggesting that the sediments were originally rich in organic matter. Calcium content of nonmineralized samples averages 28.9 wt% (i.e. approximately 72% calcite if all Ca is in calcite). At the surface, fabric-retentive dolomite is locally present with very irregular

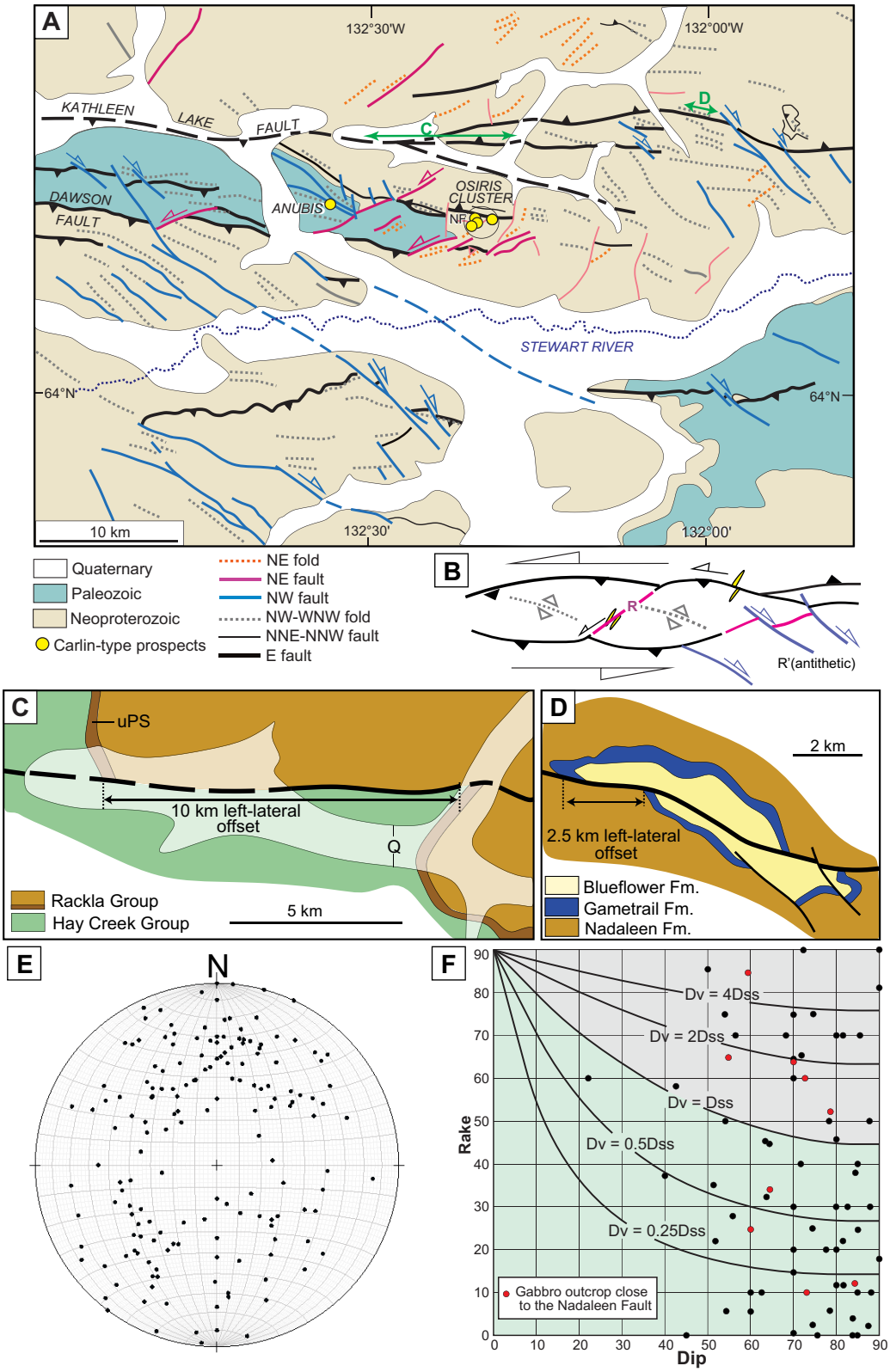

Figure 7. a) Structural framework of the eastern Rackla belt. The green arrows represent the apparent horizontal offsets along the Kathleen Lakes fault (*see* the discussion in the text). Abbreviation: NF = Nadaleen fault. **b)** Structural pattern expected in a left-lateral transpressional regime. **c and d)** Simplified geological maps showing the offsets of geological markers along the Kathleen Lakes fault system. The location is shown in Figure 7a (green arrows). *See* Moynihan (2016) for more detailed maps. Abbreviation: uPS= Sheepbed Formation. **e)** Schmidt equal-area lower-hemisphere projection of poles to bedding planes between the Kathleen Lakes fault and the Dawson Thrust/Stewart River (data are courtesy of D. Moynihan, Yukon Geological Survey). **f)** Fault-slip data were collected in the eastern Rackla belt. Abbreviations: Dss = strike-slip displacement, Dv = vertical displacement. The grey and green areas correspond to predominant down-dip and strike-slip motions, respectively.

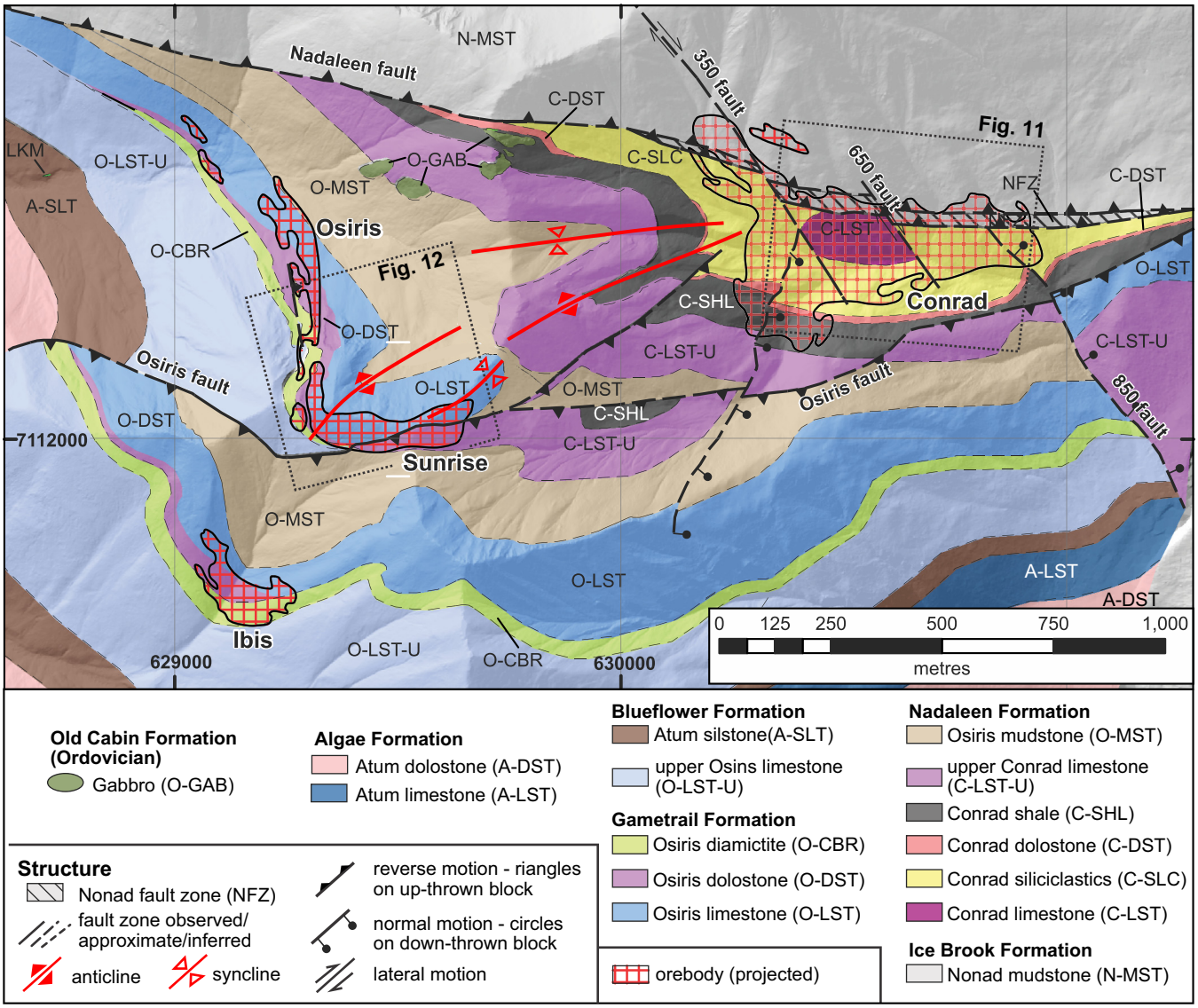

Figure 8. Geological map of the Osiris cluster area (*modified from* Steiner et al., 2018). Fold axes in the Conrad area are not shown for clarity.

dolomitization fronts. Analysis of the ATAC Resources geochemical database shows that >97% of Conrad limestone samples from the drilled area have less than 3 wt% Mg (<14% dolomite if all Mg is in dolomite), suggesting dolomitization was spatially restricted. Toward the top of the limestone unit, close to the contact with stratigraphically overlying siliciclastic rocks, the succession is more diverse. The upper part of the limestone unit is more finely laminated and includes light grey to black lime mudstone (Fig. 9e), intraclastic packstone, floatstone, and calcareous siltstone. Floatstone intervals (Fig. 9d) correspond to matrix-supported sedimentary breccia with angular fragments of lime mudstone, which are interpreted as debris flow deposits formed on a carbonate slope. The limestone unit is stratigraphically overlain by a siliciclastic unit locally known as the Conrad siliciclastics. It corresponds to grey-green siltstone and mudstone with some poorly sorted matrix-supported polymictic conglomerate with quartz pebbles (Fig. 9c) and a few weakly calcareous, centimetre-thick sandstone layers. Conglomeratic intervals up to 20 m thick are in gradational contacts with finer siliciclastic rocks and commonly exhibit synsedimentary deformation features. Pyrite (locally >2 vol.%) is disseminated throughout the unit. Both the Conrad limestone and the stratigraphically overlying Conrad siliciclastic rocks in the footwall of the fault are correlated with the Nadaleen Formation (Moynihan et al., 2019).

West of the Conrad mineralized zone, Neoproterozoic sedimentary units are cut by the Middle Ordovician Osiris gabbro that forms a 400 by 250 m intrusive body (Fig. 8; Tucker, 2015). Two 0.25–4 m thick dykes, also with gabbroic composition, are intersected in drill cores, in the footwall of the Nadaleen fault. These dykes, known as the Conrad dykes, are gabbroic and

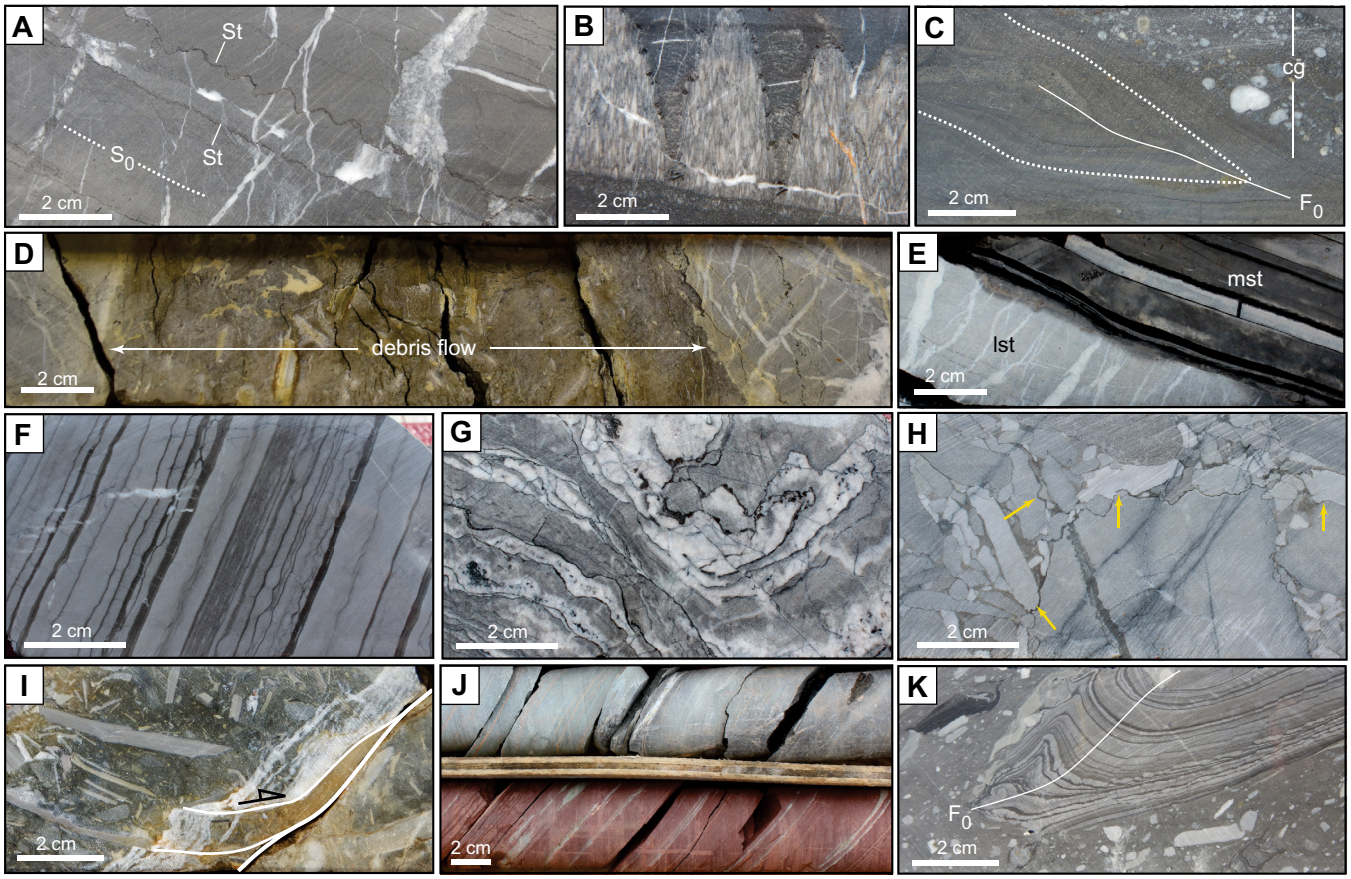

Figure 9. Photographs showing some of the lithological features of the Neoproterozoic succession in the eastern Rackla belt: a to e) Conrad area; f to k) Sunrise-Osiris area. **a)** Typical lime mudstone/packstone of the Nadaleen Formation (Conrad limestone). Abbreviations: S_0 = bedding, St = stylolite. **b)** Cone-in-cone calcite within lime mudstone of the Nadaleen Formation (Conrad limestone). **c)** Siltstone with synsedimentary folding (left part) and conglomerate with rounded to subrounded quartz clasts from the Nadaleen Formation (Conrad siliciclastic rocks). Abbreviations: cg = conglomerate, F_0 = synsedimentary fold. **d)** The floatstone interval is interpreted to have formed through debris flow within the limestone, close to the contact with the overlying siliciclastic rocks. **e)** Alternating veined lime packstone and mudstone within the Conrad limestone, close to the contact with overlying siliciclastic rocks. Abbreviations: lst = limestone, mst = mudstone. **f)** Typical lime-mudstone of the Gametrail Formation (Osiris limestone) with diagenetic stylonodular texture. **g)** Fabric-destructive dolomite within the Gametrail Formation. **h)** Clast-supported rudstone of the Gametrail Formation characterized by elongate clasts of lime mudstone. Note the indentation contacts between the clasts (yellow arrows). **i)** Floatstone interval within the Gametrail Formation. The basal contact is interpreted as a shear surface formed during debris flow emplacement. **j)** Typical varicoloured mudstone and siltstone from the Osiris mudstone. **k)** Matrix-supported polymictic conglomerate with a large clast exhibiting synsedimentary deformation.

composed of plagioclase, clinopyroxene, and secondary carbonate and pyrite. Tucker (2015) pooled five LA-ICP-MS U-Pb zircon analyses from two samples to calculate an emplacement age for the dykes of 74.1 ± 1.0 Ma. Dykes are commonly mineralized (Au >1 g/t) and contain realgar and fluorite. The inferred emplacement age of the dykes provides a maximum age limit for mineralization (Tucker et al. 2018; *see* discussion in Pinet et al., 2020).

The Nadaleen fault is the main structural feature in the Conrad area. It is an east-striking, steeply north-dipping (65º) fault with a damage zone that ranges from a few metres thick to up to several tens of metres between the north-northwest-trending 350 and 650 faults (Fig. 8). The Nadaleen fault zone records a polyphase structural history and is characterized by brittle to ductile fabrics (Fig. 10a) with kinematic indicators showing both strike-slip (predominantly left-lateral) and dip-slip (predominantly thrust) components. Most of the deformation predates mineralization, but in a few cases late- to post-mineralization displacement is documented by the offset of calcite veins with realgar and by minor fault planes with striated realgar coating. The Nadaleen fault is cut by a series of north-northwest-trending faults with apparent right-lateral displacement. Fault intersection zones show increased fracture density and mineralized intervals, but the timing of fracture permeability enhancement remains poorly constrained and both pre- and synmineralization fractures are possibly present (Pinet et al., 2020).

Though the limestone host unit is poorly exposed, there is evidence for complex folds and faults. In some cases, outcrop- to core-scale folds are a result of soft-sediment deformation (Fig. 9c). However, the radial

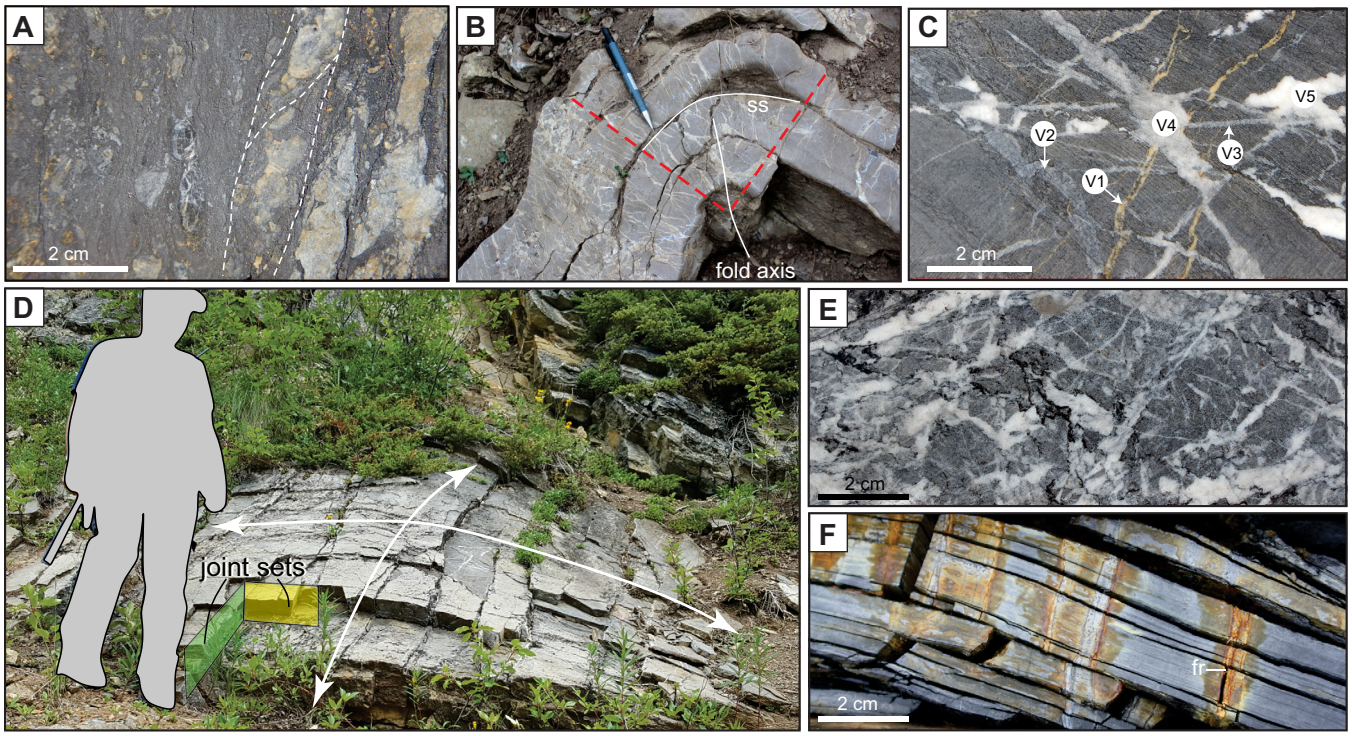

Figure 10. Photographs illustrating some tectonic features of the Neoproterozoic succession in the eastern Rackla belt. **a)** Typical brittle-ductile fabrics within the Nadaleen fault zone. Dashed lines show the main fabrics. **b)** Steeply plunging fold in the Conrad area. Note the fanning of veins (red dashed lines), suggesting that the veins are genetically associated with folding. Abbreviation: ss = slip surface. **c)** Multiple vein sets within the Conrad limestone. Crosscutting relationships allow identification of five vein generations (V_1 to V_5). **d)** Subperpendicular joint sets within the Conrad limestone. **e)** Irregular calcite veining within the Conrad limestone. **f)** A fracture that has developed perpendicular to the bedding. Note the oxidation halo around the fractures, suggesting fluid flow. Abbreviation: fr = fracture.

pattern of calcite veins in the hinge zones (Fig. 10b) clearly indicates a tectonic origin for at least some of the folds.

The deformation style at the Conrad zone varies with rock competency. In the more massive and competent intervals, multiple generations of calcite (± dolomite/quartz) veins locally represent up to 25 vol.% of the rock (Fig. 10e). Based on crosscutting relationships, up to four vein generations can be defined in hand samples (Fig. 10c), the latest generation is commonly characterized by coarse rhombohedral calcite crystals associated with realgar. Stylolites are locally well developed in thick-bedded limestone horizons (Fig. 9a). Early, bedding-parallel stylolites are the most common, but late stylolites crosscutting bedding are also present. In more thinly bedded and less competent intervals, shearing on bedding planes and bed-restricted joints predominate (Fig. 10f). Joint spacing varies from bed to bed and two well organized perpendicular joint sets are documented in outcrop (Fig. 10d).

Sunrise and Osiris Zones

The Sunrise and Osiris gold zones are located approximately 1.2 km west-southwest of the Conrad zone, on the east- and north-striking flanks of a complexly shaped anticline, respectively (Fig. 8; Steiner et al., 2018). The Sunrise and Osiris zones are in the footwall of the Osiris fault (Fig. 8). The Osiris fault is a steeply dipping (75º) fault with mixed right-lateral and reverse-sense of motion (*see* Pinet and Sack, 2019 for additional details).

Stratigraphic units in the Sunrise area (Fig. 8) have been described in Pinet and Sack (2019) and only a brief summary is given here. The oldest unit is limestone-dominated (alternating lime-mudstone and intraclastic packstone) and is locally known as the upper Conrad limestone. The upper Conrad limestone also includes a few weakly calcareous mudstone intervals and polymictic matrix-supported conglomerate with subrounded clasts. A finely (mm to a few cms) laminated varicoloured (brown, grey, green, purple) non-calcareous mudstone and siltstone unit (Fig. 9j; Osiris mudstone) stratigraphically overlies the upper Conrad limestone. This mudstone unit contains up to 3 vol.% of fine-grained pyrite and exhibits textures typical of soft-sediment deformation (Fig. 9k). Both the non-mineralized upper Conrad limestone and Osiris mudstone are part of the Nadaleen Formation (Moynihan et al., 2019). The unit that hosts the mineralization at Sunrise and Osiris corresponds to a 130 m thick limestone interval, locally known as the Osiris limestone, and has

been correlated with the Gametrail Formation of the Windermere Supergroup (Aitken, 1989; Moynihan et al., 2019). This unit is a medium grey lime-mudstone with bed thickness varying between 1 and 80 mm (average 8 mm). Some intervals show only a weak reaction to dilute (10 vol.%) HCl, indicating partial, fabric-retentive dolomitization.

The Osiris limestone also includes intraclastic rudstone and floatstone intervals interpreted as mass transport complexes resulting from different processes (short-distance translational sliding on a moderate slope and debris flows, respectively; Pinet and Sack, 2019). The rudstone intervals correspond to decimetre- to metre-thick clast-supported conglomerate with elongated lime-mudstone fragments showing stylolitic and indented contacts (flat-pebble conglomerate; Fig. 9h; Myrow et al., 2004). The floatstone intervals consist of poorly sorted polymictic, matrix-supported sedimentary breccia with variable matrix content and angular lime-mudstone clasts with variable colours and laminations (Fig. 9i). In the Osiris area (Fig. 8), a coarse-grained fabric-destructive dolostone with irregular dolomite veins (Fig. 9g; Beaton, 2015) overlies the Osiris limestone. In the Osiris limestone, multiple generations of calcite veins are documented, but they make up a smaller volume of the rock than in the Conrad limestone (Pinet and Sack, 2019).

DISCUSSION

At the regional scale, the Nadaleen trend exhibits two characteristics that have been identified as critical parameters for the formation of Carlin-type deposits in Nevada (Cline et al., 2005; Muntean, 2018a): 1) proximity to a long-lived, deep-seated tectonic feature (Dawson fault); and 2) a host sedimentary succession that includes carbonate and carbonaceous sedimentary rocks deposited in slope and base-of-slope settings. However, the spatial and temporal relationship of Carlin-type mineralized zones with magmatism (Muntean et al., 2011) remains equivocal in central Yukon because Late Cretaceous to Cenozoic igneous rocks is restricted to volumetrically minor stocks and dykes. A composite, positive magnetic anomaly with values up to 200 nT above the regional magnetic field is located 20 km west-northwest of the Conrad zone (M1 on Fig. 3) and may represent a large buried intrusion. Euler decomposition of the anomaly gives an estimate of 1.7 km for the depth of the uppermost part of the magnetic source and thus possibly the top of the intrusion. This interpretation is, however, not unique and the magnetic anomaly could also be associated with buried high magnetic susceptibility Paleoproterozoic to Mesoproterozoic sedimentary rocks. On high-resolution data flown for ATAC Resources, the residual total magnetic field also includes a low-amplitude (<50 nT) oval-shaped magnetic low centred 3.5 km southwest of the Sunrise zone. This anomaly could hypothetically be associated with a reduced (ilmenite series) intrusion.

In central Yukon, the sedimentary succession is complexly faulted and folded with several phases of deformation, but the ages of deformation are poorly constrained. Despite uncertainty about the timing and detailed kinematics of deformation phases, a regional-scale Late Cretaceous extensional event comparable to the Eocene-Miocene basin-and-range extension of the southwestern United States is not evident in the regional geology of east-central Yukon (Nelson et al., 2013). Importantly, synmineralization extension, if any, must have been kinematically linked with significant strike-slip motion along faults and not to a regional-scale episode of extension, for which no evidence has been found.

At the mineralized-zone scale, the dip (commonly >50º) of units hosting mineralization is significantly steeper than in most deposits of Nevada where shallowly dipping (<30º) favourable strata channelled mineralizing fluid out of high-angle faults contributing to the formation of tree-like mineralized envelopes (Rhys et al., 2015; Muntean, 2018a). Considering the remaining uncertainties about the exact timing of deformation and local evidence for late- to post-mineralization faults in the Osiris cluster area (fault planes with striated realgar, minor faults cutting calcite-realgar veins, and possibly brittle faults surrounding mineralized intervals in the Nadaleen fault zone), it is possible that folds may have been tightened after gold deposition and that the present-day geometry is not the same as during mineralization. However, the shape of gold-bearing mineralized bodies at Conrad strongly suggests that without the tight anticline geometry (Fig. 11) and the caprock integrity of siliciclastic intervals stratigraphically or structurally above limestone units hosting mineralization (Conrad siliciclastic units and NONAD mudstone), fluids would have escaped and may not have formed significant gold accumulations. In the Sunrise and Osiris zones, caprock units vary (Fig. 12) and correspond to the Osiris fault zone (including a 10 m thick Osiris mudstone interval) in the Sunrise area and to the Osiris dolostone in the Osiris area. In this latter case, irregular dolomite veins formed during sedimentary burial, with no evidence of younger hydrothermal fluid circulation, confirming that the dolostone, even if intensively veined, acted as an impermeable unit.

IMPLICATIONS FOR EXPLORATION

Maximum burial conditions recorded along the northern boundary of the Selwyn Basin decrease from greenschist facies in the west (Abbott, 1997) to the

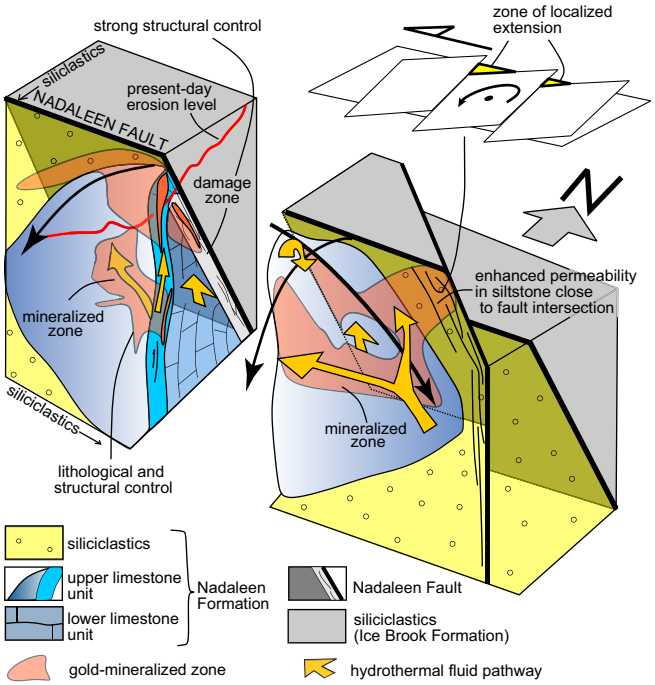

Figure 11. Schematic 3-D view of the Conrad zone.

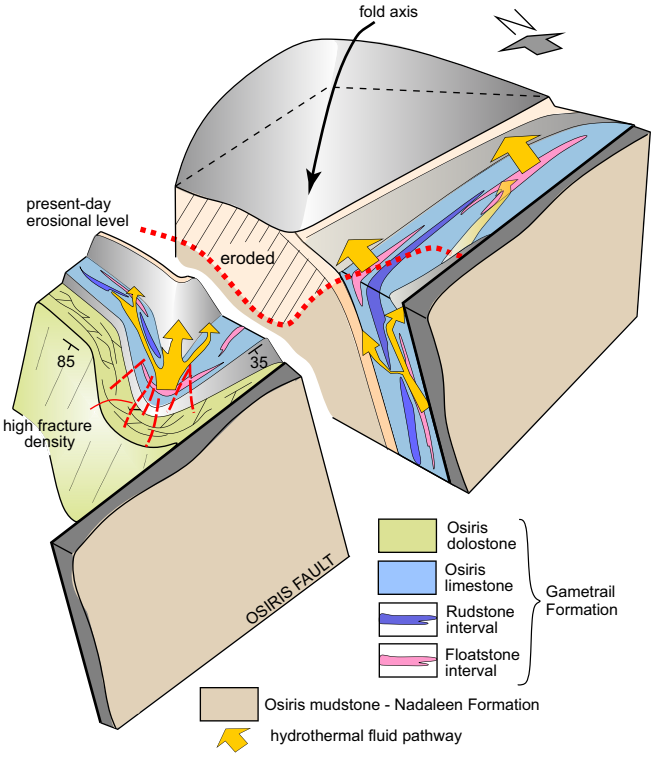

Figure 12. Schematic 3-D view of the Sunrise and Osiris zones.

anchizone in the eastern Rackla belt. In this latter area, Rock-Eval pyrolysis analyses done during this study (not shown) indicate that the kerogen present in organic-rich sedimentary rocks has lost almost all generative hydrocarbon potential (dry gas zone). The timing of differential exhumation is poorly constrained. However, if exhumation is syn- to post-mineralization, it may have resulted in the erosion of shallowly formed deposits, such as Carlin-type, in the western part of the Ogilvie platform-Selwyn Basin transition zone and their preservation in the eastern part.

The strike-slip component of motion along many of the structures that mark the northern boundary of the Selwyn Basin indicates that the detailed geometry in the map view of the main faults merits further consideration. In particular, areas characterized by a change in strike (bend) and/or step over (relay zones) may correspond to favourable zones of fluid flow and/or traps as they have the significant vertical connectivity necessary for tapping relatively deep fluid (and metal) reservoirs. Horsetail-style structures (i.e. fault that split into several branches) and fault intersections should also be considered as highly favourable zones due to the typical increase of second-order faults in these areas. Recognition of such zones may, however, be challenging, as the expression of intersecting small-displacement faults may be subtle on regional maps or regional magnetic surveys. The Conrad zone, where north-northwest-trending faults cut the Nadaleen fault is an example of such a highly favourable setting with enhanced permeability (increased density of pre- and/or synmineralization fractures and possibly localized zones of extension; Fig. 11; Pinet et al., 2020).

Several northeast-striking faults are present throughout the Nadaleen trend. Analysis of high-resolution aeromagnetic data suggests that most of these faults exhibit an apparent left-lateral sense of motion and offset more west-trending structures (Fig. 7). Interestingly, the spatial association between northeast-trending faults and latest Cretaceous mineralization (porphyry Mo and Cu systems, Ag-rich polymetallic veins, carbonate replacement, and skarn bodies) has been documented west of the Tintina fault, >350 km from the Nadaleen trend, where they exhibit left-lateral oblique extensional motion (Allan et al., 2013). East of the Tintina fault, mineralization of the Keno Hill district is also associated with northeast-trending faults with gently plunging slickenlines (D_3 of Craggs et al., 2010). Detailed structural analysis and better timing constraints should make it possible to test the potential relationship between motion on northeast-trending faults and a distinct, possibly short-duration, geodynamic event.

In the eastern Rackla belt, most of the first-order structures formed and/or have been reactivated in a regional left-lateral transpressional regime (Fig. 7b). However, the Nadaleen trend is characterized by 'anomalous' geological features that are not compatible with such a tectonic regime. These features include northeast-trending folds, the Osiris fault that exhibits

an apparent right-lateral component of motion, and the west- to northwest-trending Conrad dykes. It is presently unclear if northeast-trending folds, the motion of the Osiris fault, and intrusion of the Conrad dykes are contemporaneous. However, these structures are kinematically compatible with a west-southwest maximum principal compressive stress and there is a possibility that they represent a single 'late' structural event, hypothetically synchronous with mineralization. These late-stage structures, which post-date the main deformation event, may be significant for Carlin-type mineralization exploration in Yukon.

ACKNOWLEDGMENTS

This contribution is dedicated to Julia Lane who was instrumental in designing the project and conducting its various field and analytical components. Her help and enthusiasm are sincerely missed. Thanks to ATAC Resources for access to drill cores and data, and for logistical support and scientific input. This report beneficiated from discussions with A. Coulter, J. Ryan, and D. Moynihan (who shared the structural data presented in Fig. 7c). Y. Kuiper, C. Lawley, and R. Carne are acknowledged for their constructive reviews.

REFERENCES

Abbott, G., 1997. Geology of the upper Hart River area, eastern Ogilvie Mountains, Yukon Territory (116A/10, 116A/11); Yukon Geological Survey, Bulletin 9, 92 p.

Aitken, J.D., 1989. Uppermost Proterozoic formations in central Mackenzie Mountains, Northwest Territories; Geological Survey Canada, Bulletin 368, 26 p.

Allan, M.M., Mortensen, J.K., Hart, C.J.R., Bailey, L.A., Sanchez, M.G., Ciolkiewicz, W., McKenzie, G.G., and Creaser, R.A., 2013. Magmatic and metallogenic framework of west-central Yukon and eastern Alaska; *in* Tectonics, Metallogeny, and Discovery: The North American Cordillera and similar accretionary settings, (ed.) M. Colpron, T. Bissig, B.G. Rusk, and J.F.H. Thompson; Society of Economic Geologists, Special Publication 17, p. 111–168.

Amaru, M.L., 2007. Global travel time tomography with 3-D reference models; Ph.D. thesis, Utrecht University, Geologica Ultraiectina, v. 274, 174 p.

Arehart, G.B., Ressel, M., Carne, R., and Muntean, J., 2013. A comparison of Carlin-type deposits in Nevada and Yukon; *in* Tectonics, Metallogeny, and Discovery: The North American Cordillera and similar accretionary settings, (ed.) M. Colpron, T. Bissig, B.G. Rusk, and J.F.H. Thompson; Society of Economic Geologists, Special Publication 17, p. 389–401.

Beaton, N.I., 2015. Diagenetic controls on hydrothermal fluid flow in the Osiris, Isis and Isis East Carlin-type showings, Nadaleen trend, Yukon; M.Sc. thesis, University of Alberta, Edmonton, Alberta, 180 p.

Bineli Betsi, T., Lentz, D., Chiaradia, M., Kyser, K., and Creaser, R.A., 2013. Genesis of the Au-Bi-Cu-As, Cu-Mo±W, and base-metal Au-Ag mineralization at the Mountain Freegold (Yukon, Canada): constraints from Ar-Ar and Re-Os geochronology and Pb and stable isotope compositions; Mineralium Deposita, v. 48, p. 991–1017.

Cathro, R.J., 2006. Great mining camp of Canada- 1. The history and geology of the Keno Hill Silver camp, Yukon Territory; Geosciences Canada, v. 33, p. 103–134.

Cecile, M.P., 1982. The Lower Paleozoic Misty Creek Embayment, Selwyn Basin, Yukon and Northwest Territories; Geological Survey of Canada, Bulletin 335, 78 p.

Cline J.S., Hofstra A., H., Muntean J.L., Tosdal R.M., and Hickey K.A., 2005. Carlin-type gold deposits in Nevada: critical geologic characteristics and viable models; *in* Economic Geology 100th Anniversary Volume, (ed.) J.W. Hedenquist, J.F.H. Thompson, R.J. Goldfarb, and J.P Richards; Society of Economic Geologist, p. 541–484.

Colpron, M., 2012. Preliminary observations on the geology of the Rackla belt, Mount Ferell map area (NTS 106C/3), central Yukon; *in* Yukon Exploration and Geology 2011, (ed.) K.E. MacFarlane and P.J. Sack; Yukon Geological Survey, p. 27–43.

Colpron M., Moynihan D., Israel S., and Abbott G., 2013. Geologic map of the Rackla belt, east-central Yukon (NTS 106C/1-4, 106D/1); Yukon Geological Survey, Open File 2013-13, scale 1:50 000, 5 maps and legend.

Colpron, M., Israel, S., and Friend, M., 2016. Yukon plutonic suites; Yukon Geological Survey, Open File 2016-37, scale 1:750 000.

Craggs, S.D., Lentz, D.R., and White, J.C., 2010. Polyphase folding in the Keno Hill Ag-Pb-Zn mining district, Yukon, Canada; Expanded abstract, GeoCanada 2010, 4 p.

Davis, W.J., Pinet, N., Petts, D.C., Jackson, S.J., and Mercier-Langevin, P., 2019. U-Pb ages of hydrothermal calcite associated with Carlin-type mineralization, Nadaleen trend, north-central Yukon; Geological Association of Canada-Mineralogical Association of Canada, Volume of Abstracts, v. 42, p. 77.

Gabrielse, H., Murphy, D.C., and Mortensen, J.K., 2006. Cretaceous and Cenozoic dextral orogeny-parallel displacements, magmatism and paleogeography, north-central Canadian Cordillera; *in* Paleogeography of North American Cordillera: Evidence for and against large-scale displacements, (ed.) J.W., Haggart, R.J., Enkin, and J.W.H, Monger; Geological Association of Canada, Special Paper 46, p. 255–276.

Gordey, S.P., 1981. Structure section across south central Mackenzie Mountains, district of Mackenzie; Geological Survey of Canada, Open File 809, 1 plate.

Goodfellow, W.D. and Jonasson, I.R., 1986. Environment of formation of the Howards Pass (XY) Zn-Pb deposit, Selwyn Basin, Yukon; *in* Mineral Deposits of Northern Cordillera, (ed.) J.A., Morin; Canadian Institute of Mining and Metallurgy, Special volume 37, p. 19–50.

Hart, C.J.R., Goldfarb, R.J., Lewis, L.L., and Mair, J.L., 2004a. The northern Cordilleran Mid-Cretaceous plutonic province: Ilmenite/magnetite series granitoids and intrusion related mineralization; Resource Geology, v. 54, p. 253–280.

Hart, C.J.R., Mair, J.L., Goldfarb, R.J., and Groves, D.I., 2004b. Source and redox controls on metallogenic variations in intrusion-related ore systems, Tombstone-Tungsten belt, Yukon territory, Canada; Transactions of the Royal Society of Edinburgh, Earth Sciences, v. 95, p. 339–356.

Jeletzky, A., 1961. Eastern slope, Richardson Mountains: Cretaceous and Tertiary structural history and regional significance; *in* Geology of the Arctic, Proceedings of the first international symposium on Arctic geology, (ed) G.O., Raasch; Alberta Society of Petroleum Geologists, v. 1, p. 532–583.

Kennett, B.L.N., Engdahl, E.R., and Buland, R., 1995. Constraints on seismic velocities in the Earth from traveltimes; Geophysical Journal International, v. 122, p. 108–124.

Kingston, S., Mortensen, J.K., Gabites, J., and Dumala, M., 2010. Ar-Ar geochronology and Pb isotopic constraints on the origin

of the Rau gold-rich carbonate replacement deposit, central Yukon; *in* Yukon Exploration and Geology 2009, (ed.) K.E. MacFarlane, L.H. Weston, and L.R. Blackburn; Yukon Geological Survey, p. 213–222.

Lindsay, M.J., 2006. The structural and hydrothermal evolution of intrusion-related gold mineralization at the Brewery Creek mine, Yukon, Canada; Ph.D. Thesis, James Cook University, North Queensland, 348 p.

Macdonald, F.A., Strauss, J.V., Sperling, E.A., Halverson, G.P., Narbonne, G.M., Johnson, D.T., Kunzmann, M., Schrag, D.P., and Higgins, J.A., 2013. The stratigraphic relationship between the Shuram Carbon isotope excursion, the oxygenation of Neoproterozoic oceans, and first appearance of the Ediacara biota and bilaterian trace fossils in northwestern Canada June beds; Chemical Geology, v. 362, p. 250–272.

Macdonald, F.A., Schmitz, M.D., Strauss, J.V., Halverson, G.P., Gibson, T.M., Eyster, A., Cox, G., Mamrol, P., and Crowley, J.L., 2017. Cryogenian of Yukon; Precambrian Research, v. 319, p. 114–143.

Magnall, J.M., Gleeson, S.A., and Paradis, S., 2014. SEDEX mineralization, Macmillan Pass (Yukon): petrography, mineralogy and bulk geochemistry of the Tom and Nidd deposits; Geological Survey of Canada, Open File 7457, 37 p.

Mair, J.L., Farmer, G.L., Groves, D.I., Hart, C.J.R., and Goldfarb, R.J., 2011. Petrogenesis of postcollisional magmatism at Scheelite Dome, Yukon, Canada: evidence for a lithospheric mantle source for magmas associated with intrusion-related gold systems; Economic Geology, v. 106, p. 451–480.

Maloof, T.L., Baker, T., and Thompson, J.F.H., 2001. The Dublin Gulch intrusion-hosted gold deposit, Tombstone plutonic suite, Yukon Territory, Canada; Mineralium Deposita, v. 36, p. 583–593.

Marsh, E.E., Goldfarb, R.J., Hart, C.J.R., and Johnson, C.A., 2003. Geology and geochemistry of the Clear Creek intrusion-related gold occurrences, Tintina gold province, Yukon, Canada; Canadian Journal Earth Sciences, v. 40, p. 681–699.

Mazotti, S., and Hyndman, R.D., 2002. Yakutat collision and strain transfer across the northern Canadian Cordillera; Geology, v. 30, p. 495–498.

Meng, Q., Hooker, J., and Cartwrigth, J., 2017. Early overpressuring in organic-rich shales during burial: evidence from fibrous calcite veins in the Lower Jurassic shales with beef member in the Western Basin, UK; Journal of Geological Society, v. 174, p. 869–882.

Mortensen, J.K., Hart, C.J.R., Tarswell, J., and Allan, M.M., 2016. U-Pb zircon age and Pb isotopic constraints on the age and origin of porphyry and epithermal vein mineralization in the eastern Dawson Range, Yukon; *in* Yukon Exploration Geology 2015, (ed.) K.E. MacFarlane and M.G. Nordling; Yukon Geological Survey, p. 165–185.

Moynihan, D., 2013. Bedrock geology of NTS 106B/04, eastern Rackla belt; *in* Yukon Exploration and Geology 2017, (ed.) K.E. MacFarlane, M.G. Nording, and P.J. Sack; Yukon Geological Survey, p. 147–167.

Moynihan D., 2016. Bedrock geology compilation of the eastern Rackla belt, NTS 105N/15, 105N/16, 105O/13, 106B/4, 106C/1, 106C/2, east-central Yukon; Yukon Geological Survey, Open File 2016-2, scale 1:75 000.

Moynihan, D., Strauss, J.V., Padget, C.D., and Nelson, L.L., 2019. Upper Windermere Supergroup and the transition from rifting to continent-margin sedimentation, Nadaleen River area, northern Canadian Cordillera; Geological Society of America Bulletin, v. 131, p. 1673–1701.

Muntean, J.L., Cline, J.S., Simon, A.C., and Longo, A.A., 2011. Magmatic-hydrothermal origin of Nevada's Carlin-type gold deposits; Nature Geoscience, v. 4, p. 122–127.

Muntean, J., 2018a. The Carlin gold system: Applications to exploration in Nevada and beyond; *in* Diversity of Carlin-style Gold Deposits, (ed.) J. Muntean; Society of Economic Geologists, Reviews in Economic Geology, v. 20, p. 39–88.

Muntean, J. (ed.), 2018b. Diversity of Carlin-style gold deposits; Society of Economic Geologists, Reviews in Economic Geology, v. 20, 363 p.

Murphy, D.C., 1997. Geology of the McQuesten River region, northern McQuesten and Mayo map area, Yukon Territory (115P/14, 15, 16; 105M/13, 14); Exploration and Geological Services Division, Yukon, Indian and Northern Affairs Canada Bulletin 6, 122 p.

Myrow, P.M., Tice, L., Archuleta, B., Clark, B., Taylor, J.F., and Ripperdant, R.L., 2004. Flat-pebble conglomerate: its multiple origins and relationship to metre-scale depositional cycles; Sedimentology, v. 51, p. 973–996.

Nelson, J.L., Colpron, M., and Israel, S., 2013. The Cordillera of British Columbia, Yukon and Alaska: Tectonics and Metallogeny; *in* Tectonics, Metallogeny and Discovery: The North American Cordillera and Similar Accretionary Setttings, (ed.) M. Colpron, T. Bissig, B.G. Rusk, and J.F.H. Thompson; Society of Economic Geologists, Special Publication 17, p. 53–109.

Nelson, J.L., Paradis, S., Christensen, J., and Gabites, J., 2002. Canadian Cordillera Mississippi Valley-type deposits: A case for Devonian-Mississippian back-arc hydrothermal origin; Economic Geology, v. 97, p. 1013–1036.

Palmer, J.C. and Kuiper, Y.D., 2016. Structural geology of the eastern Nadaleen trend, Yukon Territory, Canada: Implications for recently discovered sedimentary rock-hosted gold; Ore Geology Reviews, v. 80, p. 48–60.

Pigage, L.C., 2004. Bedrock geology compilation of the Anvil district (parts of 105K/2, 3, 5, 6, 7, and 11), central Yukon; Yukon Geological Survey, Bulletin 15, 103 p.

Pilkington, M. and Saltus, R.W., 2009. The Mackenzie River magnetic anomaly, Yukon and Northwest Territories, Canada—Evidence for Early Proterozoic magmatic arc crust at the edge of the North American craton; Tectonophysics, v. 478, p. 78–86.

Pinet, N., Sack, P., Mercier-Langevin, P., Lavoie, D., Dubé, B., Lane, J., and Brake, V., 2018. Breccia styles and controls on carbonate replacement type ('Carlin type') gold zones, Rackla belt, east-central Yukon; *in* Targeted Geoscience Initiative – 2017 Report of Activities, (ed.) N. Rogers; Geological Survey of Canada, Open File 8358, p. 163–168.

Pinet, N. and Sack, P., 2019. Macroscopic control on Carlin-type gold mineralization in north-central Yukon; *in* Targeted Geoscience Initiative: 2018 report of activities, (ed.) N. Rogers; Geological Survey of Canada, Open File 8549, p. 89–103.

Pinet, N., Sack, P., Mercier-Langevin, P., Davis, W.J., Lavoie, D., Haeri-Ardakani, O., Komaromi, B.A., Dubé, B., Cline, J.S., Petts, D.C., Jautzy, J., Jackson, S.E., Percival. J.B., Savard, M.M., and Brake, V.I., 2020. Neoproterozoic-hosted Carlin-type mineralization in central Yukon, part 2: Mineralization; *in* Targeted Geoscience Initiative 5: Contributions to the Understanding of Canadian Gold Systems, (ed.) P. Mercier-Langevin, C.J.M. Lawley, and S. Castonguay; Geological Survey of Canada, Open File 8712, p. 299–314. doi:10.4095/326047

Rasmussen, K.L., 2013. The timing, composition, and petrogenesis of syn- to post- accretionary magmatism in the northern Cordilleran miogeocline, eastern Yukon and southwestern Northwest Territories; Ph.D. thesis, University of British Columbia, Vancouver, British Columbia, 788 p.

Rhys, D., Valli, F., Burgess, R., Heitt, D., Griesel, G., and Hart, K., 2015. Controls of fault and fold geometry on the distribution of

gold mineralization on the Carlin trend; Geological Society of Nevada, New Concepts and Discoveries: 2015 Symposium Proceedings, p. 333–389.

Ristorcelli, S., Ronning, P., Martin, C., and Christensen, O., 2018. Technical report and estimate of mineral resources for the Osiris project, Yukon, Canada, Mine Development Associates for ATAC Resources Ltd. <https://www.atacresources.com/assets/img/Osiris_Resource_Estimate_and_Technical_Report_2018.pdf> [accessed October 30, 2019]

Selby, D. and Creaser, R.A., 2001. Late and mid-Cretaceous mineralization in the northern Canadian Cordillera: Constraints from Re-Os molybdenite dates; Economic Geology, v. 96, p. 1461–1467.

Sinclair, A.J., Tessari, O.J., and Harakal, J.E., 1980. Age of Ag–Pb–Zn mineralization, Keno Hill – Galena Hill area, Yukon Territory; Canadian Journal of Earth Sciences, v. 17, p. 1100–1103.

Steiner, A., Hickey, K., and Coulter, A., 2018. The structural framework for Carlin-type gold mineralization in the Nadaleen trend, Yukon; *in* Yukon Exploration and Geology 2017, (ed.) K.E. MacFarlane; Yukon Geological Survey, p. 139–149.

Thiessen, E.J., Gleeson, S.A., Bennett, V., and Creaser, R.A., 2016. The Tiger deposit: a carbonate-hosted, magmatic-hydrothermal gold deposit, central Yukon, Canada; Economic Geology, v. 111, p. 421–446.

Thorkelson, D.J., Mortensen, J.K., Davidson, G.J., Creaser, R.A., Perez, W.A., and Abbott, J.G., 2001. Mesoproterozoic intrusive breccias in Yukon, Canada: the role of hydrothermal systems in reconstruction of North America and Australia; Precambrian Research, Special Volume 111, p. 31–56.

Tucker, M.J., 2015. Geology, mineralization and geochronology of the Conrad zone Carlin-type prospect, east-central Yukon Territory, Canada; M.Sc. thesis, University of British Columbia, Vancouver, British Columbia, 160 p.

Tucker, M.J., Lane, J.C., and Hart, C.J.R., 2018. Overview of Carlin-type prospects of the Nadaleen trend: A Yukon analogue to Carlin-type gold mineralization of the Great Basin; *in* Diversity of Carlin-style Gold Deposits, (ed) J. Muntean; Society of Economic Geologists, Reviews in Economic Geology, v. 20. p. 235–256.

Yeo, G.M., 1986. Iron formation in the late Proterozoic Rapitan Group, Yukon and Northwest Territories; *in* Mineral Deposits of the northern Cordillera, (ed.) J.A., Morin; Canadian Institute of Mining and Metallurgy, Special Volume 37, p. 142–153.

Yukon Geological Survey, 2019. Yukon Digital Bedrock Geology. Yukon Geological Survey. <http://data.geology.gov.yk.ca/Compilation/3> [accessed October, 2019]